Article

Fabricating Pt/Sn-In2O3 Nanoflower with Advanced Oxygen Reduction Reaction Performance for High-Sensitive MicroRNA Electrochemical Detection

Kai Zhang, HaiFeng Dong, Wenhao Dai, Xiangdan Meng, Huiting Lu, Tingting Wu, and Xueji Zhang

Anal. Chem., **Just Accepted Manuscript** • DOI: 10.1021/acs.analchem.6b02858 • Publication Date (Web): 06 Dec 2016

Fabricating Pt/Sn-In_2O_3 Nanoflower with Advanced Oxygen Reduction Reaction Performance for High-Sensitive MicroRNA Electrochemical Detection

Kai Zhang,[†] Haifeng Dong,[†,*] Wenhao Dai,[†] Xiangdan Meng,[†] Huiting Lu,[‡] Tingting Wu,[†] Xueji Zhang[†,*]

[†]Research Center for Bioengineering and Sensing Technology, School of Chemistry and Bioengineering, University of Science & Technology Beijing, Beijing 100083, P.R.China

[‡]Department of Environmental Science and Engineering, School of Chemistry and Environment, Beijing University of Aeronautics &Astronautics, Beijing 100083, P.R. China

Corresponding Author

*E-mail: hfdong@ustb.edu.cn. Fax: 86-108-237-5840

*E-mail: zhangxueji@ustb.edu.cn. Fax: 86-108-237-6993

ABSTRACT: Herein, an efficient electrochemical tracer with advanced oxygen reduction reaction (ORR) performance was designed by controllably decorating platinum (Pt) (diameter, 1 nm) on the surface of compositionally tunable tin-doped indium oxide nanoparticle (Sn-In_2O_3) (diameter, 25 nm), and using the Pt/Sn-In_2O_3 as electrochemical tracer and interfacial term hairpin capture probe, a facile and ultrasensitive microRNA (miRNA) detection strategy was developed. The morphology and composition of the generated Pt/Sn-In_2O_3 NPs were comprehensively characterized by spectroscopic and microscopic measurements, indicating numerous Pt uniformly anchored on the surface of Sn-In_2O_3. The interaction between Pt and surface Sn as well as high Pt (111) exposure resulted in the excellent electrochemical catalytic ability and stability of the Pt/Sn-In_2O_3 ORR. As proof-of-principle, using streptavidin (SA) functionalized Pt/Sn-In_2O_3 (SA/Pt/Sn-In_2O_3) as electrochemical tracer to amplify the detectable signal and a new interfacial term hairpin probe for target capture probe, a miRNA biosensor with a linear range from 5 pM to 0.5 fM and limit of detection (LOD) down to 1.92 fM was developed. Meanwhile, the inherent selectivity of the term hairpin capture probe endowed the biosensor with good base discrimination ability. The good feasibility for real sample detection was also demonstrated. The work paves a new avenue to fabricate and design high-effective electrocatalytic tracer, which have great promising in new bioanalytical applications.

INTRODUCTION

MicroRNA (miRNA), approximately 19-23 nucleotides, is a class of endogenous, non-coding short RNA molecules[1-3] that primarily act as post-transcriptional regulators of gene expression by hindering protein translation or depredating message RNA in a broad range of animals, plants, and viruses.[4-6] Especially, it has been found that the aberrant expression of miRNA is associated with a variety of cancers, genetic disorder and immune inefficiency[7-9] Therefore, miRNAs are emerging as a new type of clinically diagnostic and prognostic biomarkers and potential therapy target for new drug discovery.[10-12] However, the miRNA detection is still challenging due to the unique characterisics of miRNA including small size, low abundance and similar sequence among homogenous family. Conventional miRNA analysis methods, including the real time reverse transcription polymerase chain reaction (RT-PCR), northern blotting, and microarray technology, have different inherent shortcomings, such as low sensitivity, false positive signal and expensive equipment.[13-15] Various rapid, sensitive and reliable miRNA detection strategies are in urgent need for in vitro[16-20] or in situ miRNA analysis.[21,22]

The inherent advantages of electrochemical methods including high sensitivity, facility, cost-effective and good compatibility with microfabrication technology, attracting intense attention in nucleic analysis. To amplify the hybridization signal, various electrocatalytic enzyme-labels[22-23] and electroactive nanoparticles (NP)[24-27] were employed to construct electrochemical nucleic acid biosensors. Among these methods, NP-based electrochemical-signal amplification platform is promising due to their large surface area, excellent conductivity, good biocompatibility and stability as well as advanced catalytic properties.[28,29] For example, a highly sensitive miRNA electrochemical biosensor was developed by using metal ion functionalized titanium phosphate nanoparticles as tracer.[30] Pt NPs is the most effective candidate acting as mimic enzyme in a wide range of reaction,[31] for example, Pt NP has been widely used in CO oxidation,[32] oxygen reduction reaction[33] and hydrogen evolution reaction,[34] but it also suffers from som deficiencies such as the rare natural abundance and instability.

On the other hand, increasing the quantity of NPs in each binding event to amplify the transduction of the recognition events, thus improving the sensitivity of electrochemical detection is another major approach. For example, a SA-functionalized carbon nanotube decorated with considerable silver-nanoparticles has been designed as tracer for ultrasensitive multiplexed measurements of tumor markers.[35] Our group has developed a novel nanoparticle label of poly(styrene-co-acrylic acid) microbeads with numerous CdTe quantum dots to amplify the electrochemical signal of DNA hybridization, leading to a high sensitive electrochemical DNA biosensor.[36]

For Pt NPs, Pt supported on carbon is still the most widely used catalyst, whilst oxide supports acting as alternative to carbon have shown improved corrosion resistance and reduced electrochemical active area degradation rates and enhanced catalytic activity.[37-39]

Herein, tin was doped into the structure of indium oxide, and the resulting tin-doped indium oxide particles (Sn-In_2O_3) with high conductivity were used as supports for Pt. The interaction between Pt and surface Sn results in the excellent electrochemical catalytic ability and stability of the Pt/Sn-In_2O_3. Using the Pt/Sn-In_2O_3 hybrids as electrochemical tracer and a term hairpin capture probe immobilized on the gold electrode as probe, an ultrasensitive and selective electrochemical miRNA biosensor was developed. The inherent excellent catalytic activity combing with the numerous quantity of Pt decorated on Sn-In_2O_3 NPs provide a high sensitivity, while the term hairpin capture probe endows the biosensor with good capability to discriminate the base mismatch

Scheme 1. Illustration of electrochemical detection of miRNA using SA/Pt/Sn-In_2O_3 as electrochemical tracer.

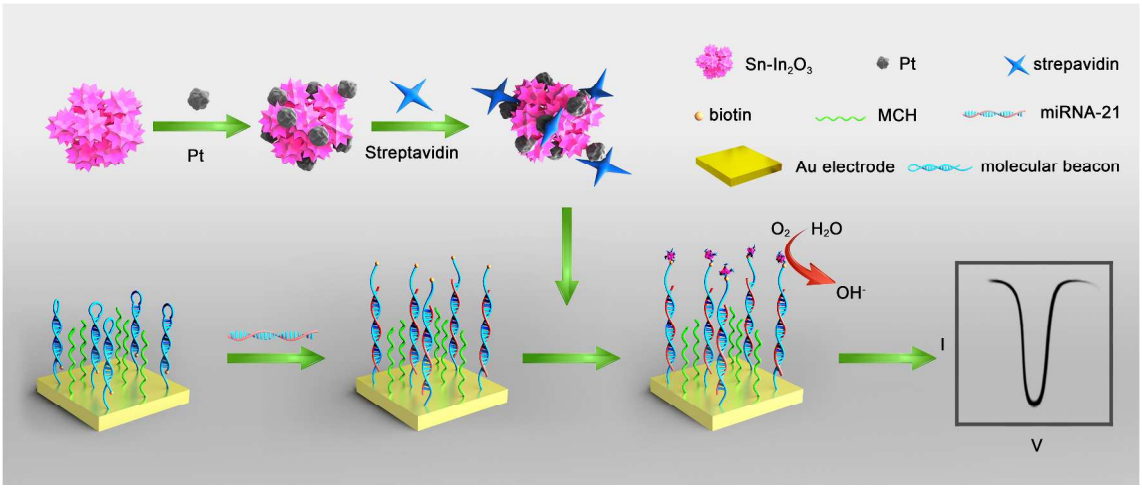

Table 1. miRNA and DNA oligonucleotides sequence used in the experiment.

Oligonucleotide	Sequence(5'---to---3')
miRNA-21	U AGC UUA UCA GAC UGA UGU UGA
term hairpin capture probe	SH-AAAAAAAAAACCTAGCATCAGTCTGATAAGCTA GCTAGG-biotin
single-base mismatched (SM) strand	U AGC UUA UCA GAC UGA UGU AGA
three-base mismatched (TM) strand	U AAC UUA UCA GAA UGA UGU AGA

Red letters, mismatched bases;

EXPERIMENTAL SECTION

Materials and Reagents. 1-(3- Dimethylaminopropyl)-3-ethylcarbodiimidehydrochloride (EDC), Tris(2-carboxy-ethyl) phosphine (TCEP), n-octylether, 6-Mercapto- 1-hexanol (MCH) were purchased from Sigma (St. Louis, MO). K_2PtCl_6 was purchased from J&K Scientific Ltd (Beijing, China). Indium(III) acetate n-octanoic acid, tin(II) 2-ethylhexanoate, and oleylamine were purchased from Xiya reagent (China). Ethylene glycol (EG) was purchased from Sinopharm Chemical Reagent Co., Ltd. (China). miRcute Plus miRNA First-Strand Cdna Synthesis Kit and miRcute Plus miRNA qPCR Detection Kit (SYBR Green) were purchased from TIANGEN (China). The stock solutions of NaH_2PO_4 (0.2 M) and Na_2HPO_4 (0.2 M) were mixed to prepare hybridization buffer (HB, 0.1 M, pH 7.0) phosphate buffered saline (PBS, 0.1 M). The pH of the HB was adjusted with NaOH (0.1 M) and H_3PO_4 (0.1M) to 7.0. The wash buffer used for removing unspecific adsorption MCH was prepared by spiking 0.05% Tween-20 into PBS (PBST). Ultrapure water (⩾18 MΩ) was obtained from a Millipore water purification system was employed in all runs. All other reagents were of analytical grade and used as received. The DNA sequence purified using high-performance liquid chromatography was from Shanghai Sangon Biological Engineering Technology & Services Co., Ltd. (China). All the RNA sequences purified using high-performance liquid chromatography were obtained from Shanghai GenePharma Co., Ltd. (Shanghai, PRC). These sequences were modifed with 2'-OMe to improve the stability. Their sequences were in **Table 1**. All the miRNA sequences were diluted in diethy pyrocarbonate (DEPC)-treated water for experiments, and all the experiments were performed in laminar flow bench to make sure the clean environment to control the influence of RNAse.

Instruments. Transmission electron microscopy (TEM) images and Energy dispersive X-ray spectroscopy (EDX) spectroscopy data were recorded on a transition electron microscope (10KVA-0.14NM, JEOL, Japan). X-ray-photoelectron spectroscopy (XPS) measurements were recorded with an ESCALAB 250 spectrometer (Thermo-VG Scientific, USA). X-ray diffraction (XRD) was recoreded by a Rigaku X-ray diffractometer with Cu KR target. Fourier transform infrared spectra (FT-IR) were recorded on Nicolet 400 Fouriertransform infrared spectrometer (Madison, WI) and electrochemical impedance spectra (EIS) was obtained with a PGSTAT30/FRA2 system (Metrohm Autolab, The Netherlands), Zeta potential analysis was measured on Nano ZS (Malvern, UK). The cyclic voltammetry (CV), linear sweep voltammograms (LSV) and differential pulse voltammetry (DPV) measurements were performed on a CHI 852B electrochemical analyzer (Co. CHI, TX) at room temperature. All measurements in electrochemical characterization of Pt/Sn-In_2O_3 were conducted on a standard cell with a Ag/AgCl (1.0 M) as reference electrode, a platinum wire as counter electrode and Pt/Sn-In_2O_3 modified glass carbon electrode, rotating disk electrode (RDE) or rotating ring disk electrode (RRDE) as the working electrode. For the miRNA biosensor, the work electrode was Au electrode (diameter = 3 mm).

Synthesis of Sn-In_2O_3 NPs. The n-octylether (10 mL) suspension of indium(III) acetate (1.04 mmol), tin(II) 2-ethylhexanoate (0.16 mmol), n-octanoic acid (3.6 mmol) and oleylamine (10 mmol) was stirred at 80 ^oC for 30 min under vacuum. The atom ratio of In to Sn was kept at 9:1. The solution was then heated at 150 ºC for 1 h under a N_2 atmosphere and stirred for the further 2 h at 280 ^oC to form the Sn-In_2O_3 nanoflowers. The products were centrifugal purification by ethanol.

Fabrication of Pt/Sn-In_2O_3 Hybrids. Firstly, 0.0525 g K_2PtCl_6 was dissolved in 40 ml EG, and the pH of solution was adjusted to 12 with 2 M NaOH in EG solvent. 0.1g Sn-In_2O_3 was then added in the above solution. Finally, the mixture was sonicated for 5 minutes and heated to 140 ^oC for 4 hours. The products were washed with a large amount of water and isolated with filtration, then dried in air.

Electrochemical Characterization of Pt/Sn-In_2O_3 Hybrids. The electrode was polished with 1 and 0.3 mm alumina powder, and then it was rinsed and sonicated with water and ethanol to remove any alumina residues, then dried under N_2 before test catalytic properties of nanocomposite. 1 mg of Pt/Sn-In_2O_3 or Pt/C sample was added into 1 mL ethanol and sonicated for at least 30 minutes to give a concentration of 1 mg/mL. 20 μL of catalyst ink was then dropped on the work electrode and dried in air, 2 μL of 5% Nafion was then dropped on the electrode and allowed to dry in air. CV was performed in O_2-saturated 0.1 M KOH solution at a scan rate of 100 mV/s ranging from -0.8 to 0.2 V. For RDE, LSV was measured in O_2-saturated 0.1 M KOH solution at a scan rate of 10 mV/s under different speeds.

Assembly of Streptavidin (SA) Functionalized Pt/Sn-In_2O_3. 1 mg/mL Pt/Sn-In_2O_3 NPs were firstly mixed with 1 mM thioglycollic acid (TGA) aqueous solution. The above mixture was placed on a shaker for 12 h and subsequently cleaned by repeated centrifugation. The carboxyl-modified Pt/Sn-In_2O_3NPs were then mixed with SA in 10 mM PBS included 10 mM EDC. The EDC acts as an amine-reactive and carboxyl zero-length crosslinker, facilitating the formation of amino bond between SA and Pt/Sn-In_2O_3 to form SA/Pt/Sn-In_2O_3. The final mixture was placed on a shaker for 2 h, and the SA/Pt/Sn-In_2O_3 were obtained by repeated centrifugation.

Fabrication of miRNA Biosensor. The gold electrode was sequentially polished with 1 and 0.3 mm alumina powder and washed thoroughly with distilled water. The electrode was then sonicated in ethanol solution and distilled water and dried with a high-purify nitrogen steam. Afterwards, the electrode was activated by a series of oxidation and reduction cycle in the solution (0.01 M KCl, 0.05 M H_2SO_4) before modified.[40]A total of 5 μL of term hairpin capture probe probe solution (50 nM) containing 2 μM TCEP in the HB solution was dropped nto the electrode surface for 16 h at room temperature. The TCEP can break disulfide bonds within and between thiol-modified DNA probes. It activates thiol groups of DNA probes to form Au-S bonds with the Au electrode and anchor the DNA probes on the surface of the Au electrode. The electrode then was washed thoroughly with PBST to remove nonspecifically bound oligonucleotides, which was then immersed in a 1 mM MCH for 1 h to block the surface. The surface was then rinsed with PBST, and 5 μL of different concentrations of target miRNA was dropped onto the resulting electrode to hybridize with the term hairpin capture probe at 37 °C for 30 min. Afterwards, the electrode was rinsed with PBST again and incubated with 5 μL solution contain SA/Pt/Sn-In_2O_3 NPs at 37 °C for 1h. After rinsing with PBST, the electrochemical signal was detected in O_2-saturated PBS (100 mM, pH 8.0). All the experiments were performed under the room temperature (25 ^oC) controlled by air conditioning system and in the atmosphere.

MiRNA Analysis in Cell Lysates. MiRNA analysis in cell lysates was performed according to our previous protocol[41] A549 cells and HeLa cells were modified Eagle's medium (DMEM), respectively. The medium was supplemented with 10% fetal bovine serum (FBS) and 1% penicillin-streptomycin, and cells were grown in a humidified incubator in 5% CO_2 and 95% air at 37 ^oC. These cells were harvested after incubation for 48 hours and washed with PBS (10 mM, pH 7.4) twice times and counted with a hemocytometer. To extract the RNA, the harvested cells were firstly recycled at 37 ^oC and liquid nitrogen for 3 min thrice times. 200 μL of PBS (10 mM, pH 7.4) and 40 μL of chloroform were then added into the solution containing the cells lysates under violent shaking for 15 s. Afterwards, the mixture was kept at room temperature for 3 minutes. Afterwards, the resulting mixture was then centrifuged at 12000 rpm for 15 minutes to collect the supernatant following by adding 100 μL of isopropanol into the supernatant. The mixture was kept at room temperature for 10 minutes. The RNA was precipitated by centrifugation at 13000 rpm for 10 minutes, and the resulting RNA was redispersed in 30 μL of DEPC-treated water and the miRNA was analyzed by the same procedure mentioned as above.

RESULTS AND DISCUSSION

Morphological and Compositional Characterizations of Pt/Sn-In_2O_3. The morphology of Pt/Sn-In_2O_3 NPs was characterized by TEM. As shown in

Figure 1 a, the Sn-In_2O_3 exhibited an uniform nanoflower morphology with a diameter of about 25 nm. After the depositing of Pt NPs, numerous small, dark contrasting spherical Pt NPs with a diameter of 1 nm was dispersed on the "leaves" of the Sn-In_2O_3 NPs (**Figure S1**), which suggested that the simple Pt direct reduction deposition could effectively produce dispersed Pt nanoparticles on the surface of Sn-In_2O_3 NPs. The high resolution TEM (HRTEM) was further employed to reveal the lattice structure. The oblivious lattice structure spacing of 0.29 and 0.18 nm associated with (222) and (440) planes of Sn-In_2O_3[42] was observed, indicating the successful synthesis of Sn-In_2O_3 NPs (**Figure 1c**). As shown in **Figure 1b**, the distinct lattice spacing of 0.228 nm are associated with (111) planes of Pt nanoparticles[43], confirming the successful fabrication of the Pt/Sn-In_2O_3. EDX analysis of Pt/Sn-In_2O_3NPs presented characteristic peaks assigned to O, In, Cu (substrate) and Sn, respectively, and an obvious peak assigned to Pt was also observed compared to Sn-In_2O_3NPs (**Figure S2**), which implied Pt NPs were successfully decorated on the Sn-In_2O_3 NPs surface (**Figure 1d**). These results demonstrated that Pt NPs could effectively and uniformly decorate on the surface of the Sn-In_2O_3 by simple hydrothermal reduction.

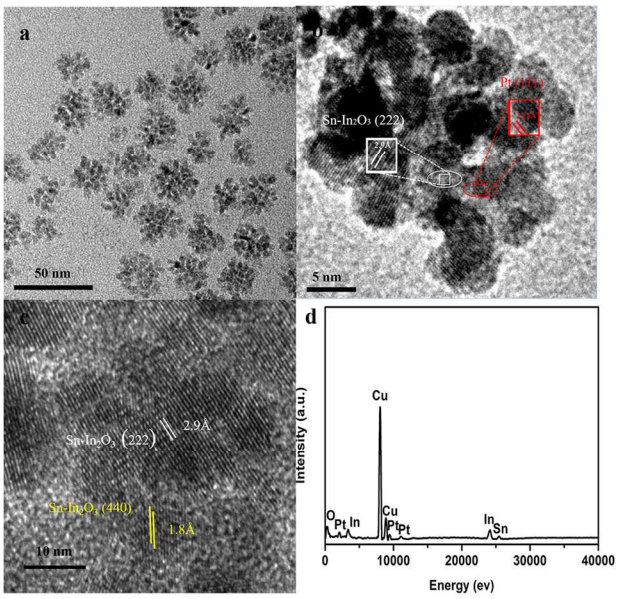

Figure 1. a) TEM image of Sn-In_2O_3 NPs, Inset shows the HRTEM image of Sn-In_2O_3 NPs. b) HRTEM image of Pt/Sn-In_2O_3 NPs. c) HRTEM image of Sn-In_2O_3 NPs. d) EDX spectrum of Pt/Sn-In_2O_3 NPs.

XRD analysis was used to investigate the crystalline structure of the as-prepared Sn-In_2O_3. The corresponding lattice spacing from the XRD analysis in **Figure 2** was consistent with **Figure 1c**, confirming the good crystalline structure of Sn-In_2O_3. As shown in **Figure 2**, the as-prepared sample exhibited the main characteristic diffraction peaks for Sn-In_2O_3. The 2θ values of 21.32°, 30.60°, 34.45°, 37.51°, 41.74°, 45.54°, 50.96°, 56.13° and 60.55° was attributed to the (211), (222), (400), (411), (322), (134), (440), (611), (622) planes of Sn-In_2O_3, respectively, and intense reflection peaks corresponding to the highly crystalline cubic bixbyite structure of In_2O_3 (ICDD PDF No. 6-416) were observed. It was concluded that tin existed as a dopant into the indium oxide lattice, and a solid solution of Sn-In_2O_3 rather than a mixture of indium oxide and tin oxide was produced due to the absence of peaks corresponding to crystalline SnO_2 phase. The characteristic peaks attributed to Pt were presented in the XRD pattern of the Pt/Sn-In_2O_3 (**Figure S3**), and the broader peaks of (411) and (322) in Pt/Sn-In_2O_3 compared to Sn-In_2O_3, indicating the Pt NPs was smaller than the Sn-In_2O_3 NPs.

The components of In_2O_3 and Pt/Sn-In_2O_3 NPs were examined by XPS analysis. As expected, the characteristic peaks related to oxygen, tin, indium, and carbon (substrate) were presented in survey spectrum of Sn-In_2O_3 **Figure 2a**, while the Pt 4f peak and pt 4d peak were observed in Pt/Sn-In_2O_3 in addition to the expected elements from Sn-In_2O_3. The high-resolution spectrum for In 3d in Sn-In_2O_3 could be deconvoluted into one doublet at 444.4eV and 452eV, corresponding with the binding energy of $In^{3+}3d_{5/2}$ and $In^{3+}3d_{3/2}$ (**Figure 2b**). Positive shift of In 3d characteristic peaks were observed in Pt/Sn-In_2O_3 (**Figure 2b**) compared to Sn-In_2O_3. As shown in **Figure 2c**, the Sn 3d XPS spectrum peak of Sn-In_2O_3 presented obvious characteristic peaks of Sn $3d_{5/2}$ and Sn $3d_{3/2}$ located at 487.1 and 495.7 eV, which could be further deconvoluted to Sn^{4+} (red dot line) and Sn^{2+} (blue dot line) states, respectively, according to the binding energy. Compared to Sn-In_2O_3, an increase of Sn^{2+} state was observed in Pt/Sn-In_2O_3. Importantly, the Sn peaks in Pt/Sn-In_2O_3 shifted positively compared to Sn-In_2O_3 (**Figure 2c**). These results suggested that the Pt/Sn-In_2O_3 catalysts exhibited a higher Sn 3d binding energy than pure SnO_2 NPs (486.70 eV)[44] due to the interaction of Sn and Pt, which indicated the formation of bond interaction between Sn and Pt.[45] As shown in **Figure 2d**, the Pt 4f peak was deconvoluted into two doublets of [Pt 1 (72.15 eV), Pt 2 (73.05 eV)] and [Pt 3 (75.45 eV), Pt 4 (76.45 eV)], which was assigned to Pt $4f_{7/2}$ and Pt $4f_{5/2}$, respectively. It revealed small shift of the Pt 4f signal toward higher binding energy compared to pure Pt,[46] which further supported the existence of a strong metal-support interaction between Pt and Sn-In_2O_3. Importantly, the interaction resulted in electron transfer between Pt and surface Sn[47], enabling good activity and stability of Pt/Sn-In_2O_3.

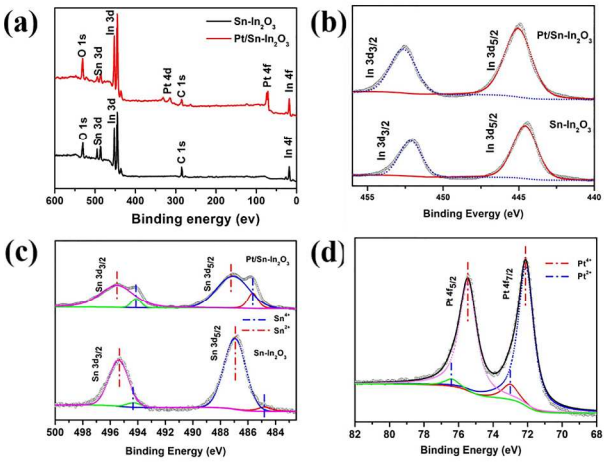

Figure 2. a) XPS survey spectra of the as-synthesized Sn-In_2O_3 and NPs Pt/Sn-In_2O_3 NPs. b) focused In 3d spectra of the as-synthesized Sn-In_2O_3 NPs and Pt/Sn-In_2O_3 NPs Pt/Sn-In_2O_3 NPs. c) focused Sn 3d spectra of the as-synthesized Sn-In_2O_3 NPs and

$Pt/Sn\text{-}In_2O_3$ NPs. d) focused pt 4f spectra of the as-synthesized $Pt/Sn\text{-}In_2O_3$ NPs.

Electrochemical Characterizations of $Pt/Sn\text{-}In_2O_3$. The CV measurements were used to investigate the catalytic property of $Pt/Sn\text{-}In_2O_3$. As shown in **Figure 3a**, the $Pt/Sn\text{-}In_2O_3$ modified electrode showed a well defined reduction peak at about -0.202 V that was competitive to the commercial Pt/C catalyst with a reduction peak at -0.2 V, suggesting a pronounced electrocatalytic activity of the $Pt/Sn\text{-}In_2O_3$ toward oxygen reduction reaction (ORR). **Figure 3b** showed the LSV response of commercial Pt/C and $Pt/Sn\text{-}In_2O_3$ catalysts. The half-wave potential of $Pt/Sn\text{-}In_2O_3$ was 35 mV that was more positive than that of Pt/C, which further confirmed the excellent ORR activity of $Pt/Sn\text{-}In_2O_3$ catalyst. These results illustrated that the superior catalytic performance of $Pt/Sn\text{-}In_2O_3$ to that of the Pt/C catalyst. As for this reason, the electronic effect between Pt and SnO_2 and a high composition of Pt (111) facets synergistically contributed to the pronounced ORR catalytic activity of the $Pt/SnO_2/C$.[48]RRDE voltammograms of the $Pt/Sn\text{-}In_2O_3$ and Pt/C in O_2-saturated 0.1 M KOH at 1600 rpm **(Figure S4)** futher indicated the good ORR catalytic activity of the $Pt/Sn\text{-}In_2O_3$**.**

RDE measurements were performed at different rotation rates (400 to 2500 rpm) with a scan rate of 10 mV s^{-1} to analyze the ORR activity and the kinetics of the proposed catalyst. The limiting current density of $Pt/Sn\text{-}In_2O_3$ electrode increased with increasing rotation speed (**Figure 3c**). The corresponding Koutecky–Levich (K–L) plots exhibited the inverse current density (j^{-1}) as a function of the inverse square root of the electrode rotation speed ($\omega^{-1/2}$) at different potential (**Inset** in **Figure 3c**). The number of electrons transferred per O_2 on the electrodes were determined by the K–L equation[49]: the linear plots suggested first-order reaction kinetics towards oxygen reduction from −0.3 to −0.6 V, over which the transferred electron number (n) per oxygen molecule involved in the Pt/ $Sn\text{-}In_2O_3$-based ORR process was calculated to be ~3.7, which indicated that Pt/ $Sn\text{-}In_2O_3$ favored predominately a four-electron oxygen reduction process and pronounced ORR catalytic activity. The stability was investigated by CV cycling test between -0.8 and 0.8 V for 300 cycles at 10 mV/s in O_2-saturated 0.1M KOH electrolyte (**Figure 3d**). There was a slight decrease current density and negligible catalytic activity reduction after 300 cycles, which revealed the excellent stability of the $Pt/Sn\text{-}In_2O_3$. The pronounced ORR catalytic activity coupling with the excellent stability of the $Pt/Sn\text{-}In_2O_3$ suggested that the $Pt/Sn\text{-}In_2O_3$ was a promising potential electrochemical tracer, which inspired us to further explore the bioanalytical application of $Pt/Sn\text{-}In_2O_3$.

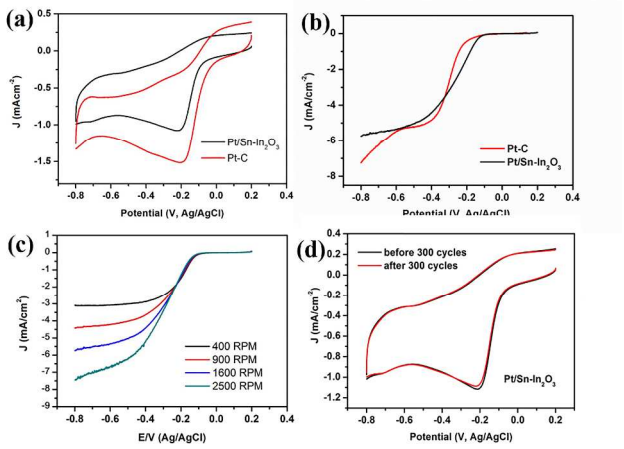

Figure 3. a) CV response of $Pt/Sn\text{-}In_2O_3$ and the commercial Pt/C catalyst, in O_2-saturated 0.1 M KOH. b) RDE voltammograms of the $Pt/Sn\text{-}In_2O_3$ and the commercial Pt/C catalyst in O_2-saturated 0.1 M KOH at 1600 rpm. c) RDE voltammograms of the $Pt/Sn\text{-}In_2O_3$ in O_2-saturated 0.1 M KOH with different electrode rotation rates. Inset a: the transferred electron numbers at different potentials. d) CV comparison of $Pt/Sn\text{-}In_2O_3$ between -0.8V and 0.2V of before and after 300 cycles in oxygen-saturated 0.1 M KOH.

Fabrication and Characterization of SA/$Pt/Sn\text{-}In_2O_3$. The $Pt/Sn\text{-}In_2O_3$ was functionalized with SA to fabricate an efficient electrochemical tracer ($SA/Pt/Sn\text{-}In_2O_3$) in bioanalysis. As shown in **Figure 4a,** the $SA/Pt/Sn\text{-}In_2O_3$ displayed larger electrochemical impedance compared to $Pt/Sn\text{-}In_2O_3$, which was resulted from the poor conductivity of SA, indicating the successful modification of SA. The FT-IR spectra were further used to characterize the $SA/Pt/Sn\text{-}In_2O_3$. In comparison with TGA functionalized $Pt/Sn\text{-}In_2O_3$, the $SA/Pt/Sn\text{-}In_2O_3$ displayed obvious absorption peaks assigned to the amide bands I (1635 cm-1) and II (1570 cm-1) of -CONH- groups attributed to the SA, confirming the formation of $SA/Pt/Sn\text{-}In_2O_3$[50]. Similar result was observed in the zeta potential analysis (**Figure 4c**). The conjugation of negative TGA to $Pt/Sn\text{-}In_2O_3$ induced positive-to-negative change of the zeta potential, while further conjugation positive SA functionalization caused a negative-to-positive change, which strongly supported the successful functionalization of SA. It was worthy to mention that the functionalization of $Pt/Sn\text{-}In_2O_3$ with TGA and SA could impart $Pt/Sn\text{-}In_2O_3$ with good solubility in aqueous solution **(Figure 4d)**, which is pivotal in bioanalysis.

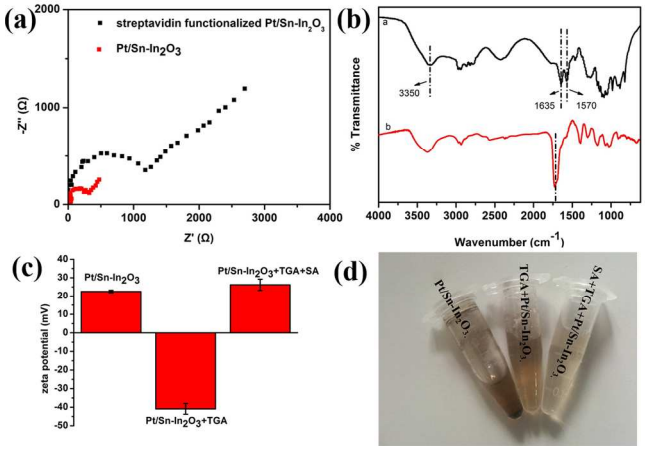

Figure 4. a) EIS Nyquist plots of $Pt/Sn\text{-}In_2O_3$ and $SA/Pt/Sn\text{-}In_2O_3$. b) FT-IR spectra of $SA/Pt/Sn\text{-}In_2O_3$ (red) and TGA functionalized $Pt/Sn\text{-}In_2O_3$ (black). c) Zeta potential characterization and d) of Photograph $Pt/Sn\text{-}In_2O_3$, TGA functionalized $Pt/Sn\text{-}In_2O_3$ and $SA/Pt/Sn\text{-}In_2O_3$

Preparation of miRNA Biosensor. As shown in **Scheme 1**, a miRNA electrochemical biosensor was developed by using the $SA/Pt/Sn\text{-}In_2O_3$ as electrochemical tracer to amplify the detectable signal and a new interfacial term hairpin capture probe for target capture probe. The term hairpin capture probe with two terminals labeled with biotin and thiol moieties, respectively, was modified on gold electrode surface via sulfur–gold interaction. In the absence of target, the term hairpin capture probe in the ''closed'' state with two terminals sequence self-complementary to form duplex structure, and the electrochemical tracer was blocked for the interaction with the biotinylated end due to the large steric effect. Up hybridization with target, the loop sequence formed a rigid duplex with the target and made the shorter stem duplex separation. Consequently, the end biotin was ''activated'' from the electrode for accessibility to electrochemical tracer, $SA/Pt/Sn\text{-}In_2O_3$, producing an electrochemical signal of oxygen reduction for detection in O_2-saturated solution.

Optimization of Experimental Conditions. The concentrations of the $SA/Pt/Sn\text{-}In_2O_3$ and term hairpin capture probe sharply influenced the performance of the biosensor, which were initially optimized. As shown in **Figure 5a**, the current intensity increased along with the increase of the concentration of term hairpin capture probe from 50 fM to 5 nM. However, the current intensity decreased when further increase of the concentration of term hairpin capture probe. It might be resulted from the large steric resistance caused by the high density of probe, and which blocked the accessibility of the target. Therefore, 5 μL of 5 nM term hairpin capture probe was selected for all the following experiments. Similarly, the concentration of $SA/Pt/Sn\text{-}In_2O_3$ was investigated. As shown in **Figure 5b**, the current intensity increased rapidly as the concentration of $SA/Pt/Sn\text{-}In_2O_3$ increased from 50 ng/ml to 50 μg/ml, and then tended to level off after 50 μg/ml. Thus, the concentration of 50 μg/ml was selected in all following experiments.

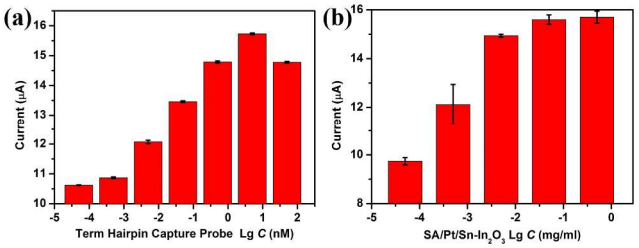

Figure 5. Influences of the concentrations of a) term hairpin capture probe (50 nM, 5 nM, 0.5 nM, 50 pM, 5 pM, 0.5 pM, 50 fM) used for preparation of modified gold electrode at 5 nM target miRNA and 0.05 mg/ml $SA/Pt/Sn\text{-}In_2O_3$ NPs. b) $SA/Pt/Sn\text{-}In_2O_3$ NPs (0.5 mg/ml, 50 μg/ml, 5 μg/ml, 0.5 μg/ml, 50 ng/ml) used for detection at 5 nM term hairpin capture probe and 5 nM target miRNA on the DPV response toward oxygen reduction.

Electrochemical miRNA Assay. Under optimized condition, after the term hairpin capture probe subsequently hybridizing with the target and recognizing with the electrochemical tracer, the electrochemical response in O_2-saturated solution was recorded. As shown in **Figure 6a**, the amplified DPV signal increased with the increasing concentration of miRNA-21. The current intensity displayed a good linear relationship with the logarithm of miRNA-21 concentration in the range from 50 pM to 5 fM. The value of the signal of the blank was -6.83 μA , and the standard deviation was 0.18. The limit of detection (LOD) was 1.92 fM at three times the standard deviation of the control (free of target miRNA). It was superior to other metal mimic enzyme-based nucleic acid detection system, such as Ag NPs with a LOD of 14 nM[51], graphene oxide–gold NPs with a LOD of 1 fM,[52] CuO NPs with a LOD of 0.73 pM.[53] It also showed enhanced sensitivity than electrocatalytic NPs tracer-based miRNA detection,[54] which was resulted from the excellent ORR catalytic capability of $SA/Pt/Sn\text{-}In_2O_3$. Moreover, we compared our approach with the gold standard qRT-PCR technique (Figure S5). The concentration of endogenous miRNA-21 detected by the electrochemical approach responded to (157.3±19.7) pM and exhibited no statistical differences (ANOVA and Tukey test, 99% confidence level) when compared with the miRNA-21 concentration measured by qRT-PCR ((289 ± 48) pM) (Figure 6b). Noticeably, the electrochemical approach showed a high precision for miRNA detection.

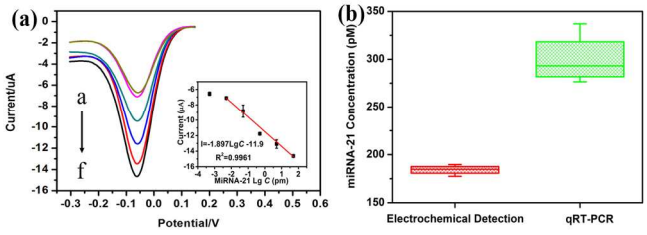

Figure 6. a) DPV response at different target concentrations. a-f: 0.5 fM,5 fM, 50 fM, 0.5 pM, 5 pM and 50 PM target miRNA. The Inset: plot of the peak current intensity versus the logarithm of target concentration in O_2-saturated PBS (100 mM, pH 8.0). b) Quantification of miRNA-21 by electrochemcal approach and qRT-PCR strategy.

Selectivity, Stability and Reproducibility. Selectivity is another important factor for a biosensor, which was tested by DPV response of our biosensor to three types of miRNA

sequences at the same concentration (5 nM), including complementary target, SM strand, and TM strand. As shown in **Figure 7**, the current intensity showed negligible change after addition of SM and TM at a concentration of 5 nM compared to the control. The complementary target exhibited a strong current intensity that was 1.83-fold and 1.91-fold higher than the intensity of the SM strand and TM mismatched strand, respectively. The high sequence selectivity may be attributed to unique essential selectivity of the term hairpin capture probe. The result suggested that the proposed assay had excellent base discrimination capability, and had potential application in single nucleotide polymorphism analysis. We further carried out a long-term cycling test to investigate the stability of the biosensor. The negligible difference of the current intensity before and after 10 cycles indicated the good stability of the biosensor (Figure 7b). Reproducibility is an important standard to evaluate the performance of the biosensor. Sample solutions including 0.5 pM and 5 pM of target miRNA-21 were used to test the reproducibility of the biosensor. Each experiment was tested 6 times, respectively. Similar current intensities were observed at the same concentration level, and the RSD value for the miRNA concentration of 0.5 pM (Figure 7c) and 5pM (Figure 7d) were 1.5% and 2%, respectively, indicating an excellent analytical reproducibility.

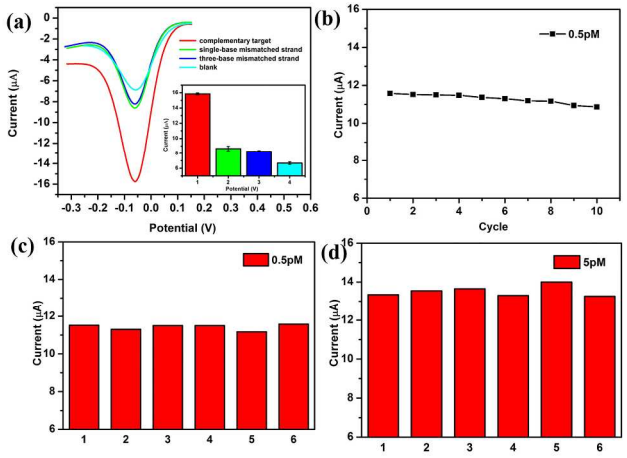

Figure 7. a) DPV response for 5 nM complementary target, SM strand, TM strand and blank in O_2-saturated PBS (100 mM, pH 8.0). Inset a: the corresponding peak currents. b) Stability test of the biosensor toward 0.5 pM target through ten cycles in O_2-saturated PBS (100 mM, pH 8.0). Current intensity of c) 0.5 pM and d) 5 pM target through 6 times replicated test in O_2-saturated PBS (100 mM, pH 8.0)

miRNA Detection in Cell Lysates. To evaluate the feasibility of the biosensor for real sample detection, the expression of miRNA in human lung adenocarcinoma cell line A549 (a cell line with high expression of miRNA-21) and human cervical cancer cell line HeLa (a cell line with low expression of miRNA-21) were investigated by using the electrochemical assay. As shown in **Figure 8a**, both of the current intensities increased when the cells amount increased from 10^3 cells to 10^6. The comparison manifested the higher expression of miRNA-21 in the A549 cells than that in the HeLa cells, which was well consistent to previous reports[55,56]. The miRNA-21 from the same sample of A549 cells was also investigated using a standard qRT-PCR (Figure S6). Compared to qRT-PCR detection, the concentration of endogenous miRNA-21 of A549 cells detected by the electrochemical approach exhibited no statistical differences (Figure 8b). Therefore the proposed electrochemistry biosensor allowed miRNA detection in real samples and had promising potential in clinical application.

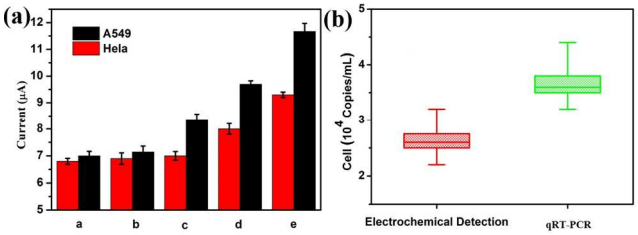

Figure 8. a) Application of the biosensor in analysis of samples coming from A549 and HeLa cell lines: (a) 10^2 cells, (b) 10^3 cells, (c) 10^4 cells, (d) 10^5 cells, and (e) 10^6 cells. DPV ignals were measured in O_2-saturated PBS (100 mM, pH 8.0) b) Quantification of miRNA-21 of A549 by electrochemcal approach and qRT-PCR strategy.

CONCLUSION

In conclusion, an efficient metal mimic enzyme of Pt/Sn-In_2O_3 possessing superb oxygen reduction catalytic property was controllably fabricated by a facile hydrothermal routine. Comprehensive microscopic and spectroscopic tools including TEM, HRTEM, XRD and XPS confirmed that Pt nanoparticles could effectively and uniformly decorate on the surface of the Sn-In_2O_3. The strong interaction between the Pt and Sn as well as the high Pt (111) exposure endows the Pt/Sn-In_2O_3 with high ORR catalytic activity. Using the SA functionalized Pt/Sn-In_2O_3 hybrids as electrochemical tracer to amplify detection signal and an interfacial term hairpin capture probe immobilized on the gold electrode as capture probe, an ultrasensitive and selective electrochemical miRNA biosensor was constructed. The high catalytic capability of Pt/Sn-In_2O_3 NPs resulted in high sensitivity, while the inherent selectivity of the term hairpin capture probe endowed the biosensor with good base discrimination ability. It also displayed pronounced precision, stability and reproducibility as well as good feasibility for real sample detection. The proposed strategy contributes to design efficient Pt-based metal mimic enzyme with high catalytic property, which hold great promise in bioanalysis.

ASSOCIATED CONTENT

Notes

The authors declare no competing financial interest.

ACKNOWLEDGMENTS

The work was supported by National Natural Science Foundation of China (Grant No.21305008, 21475008, 21275017, 21127007), Ph.D. Programs Foundation of Ministry of Education of China (No.11170197), the Fundamental Research Funds for the Central Universities (NO. FRF-BR-15-020A) and the Chinese 1000 Elites Program; State Key Laboratory of Analytical Chemistry for Life Science SKLACLS1401 and the

Special Foundation for State Major Research Programe of China (NO. 2016YFC0106602);

Supporting Information

The Supporting Information is available free of charge on the ACS Publications website.

Electrochemical analysis, TEM, EDX, XRD analysis of Pt/Sn-In_2O_3 NPs, XRD patterns for the Sn-In_2O_3, RRDE voltammograms of the Pt/Sn-In_2O_3 and Pt/C, qRT-PCR experiments

REFERENCES

(1) Mallory, A. C.; Vaucheret, H. *Nat. Genet.* **2006**, *38*, 850-850.

(2) Ha, M.; Kim, V. N. *Nat. Rev. Mol. Cell. Bio.* **2014**, *15*, 509-524.

(3)Necsulea, A.; Soumillon, M.; Warnefors, M.; Liechti, A.; Daish, T.; Zeller, U.; Baker, J. C.; Gruetzner, F.; Kaessmann, H. *Nature* **2014**, *505*, 635.

(4) Bartel, D. P. *Cell* **2004**, *116*, 281-297.

(5) He, L.; Thomson, J. M.; Hemann, M. T.; Hernando-Monge, E.; Mu, D.; Goodson, S.; Powers, S.; Cordon-Cardo, C.; Lowe, S. W.; Hannon, G. J.; Hammond, S. M. *Nature* **2005**, *435*, 828-833.

(6) He, L.; Hannon, G. J. *Nat Rev Genet.* **2004**, *5*, 522-531.

(7) Jeffrey, S. S. *Nat Biotech.* **2008**, *26*, 400-401.

(8) Esquela-Kerscher, A.; Slack, F. J. *Nat Rev Cancer.* **2006**, *6*, 259-269.

(9) Lu, J.; Getz, G.; Miska, E. A.; Alvarez-Saavedra, E.; Lamb, J.; Peck, D.; Sweet-Cordero, A.; Ebert, B. L.; Mak, R. H.; Ferrando, A. A.; Downing, J. R.; Jacks, T.; Horvitz, H. R.; Golub, T. R. *Nature* **2005**, *435*, 834-838.

(10) Koppers-Lalic, D.; Hogenboom, M. M.; Middeldorp, J. M.; Pegtel, D. M. *Adv. Drug. Deliver. Rev.* **2013**, *65*, 348-356.

(11) Ling, H.; Fabbri, M.; Calin, G. A. *Nucleic Acids Res.* **2013**, *12*, 847-865.

(12) Lujambio, A.; Lowe, S. W. *Nature* **2012**, *482*, 347-355.

(13) Li, J.; Yao, B.; Huang, H.; Wang, Z.; Sun, C.; Fan, Y.; Chang, Q.; Li, S.; Wang, X.; Xi, J. *Anal. Chem.* **2009**, *81*, 5446-5451.

(14) Yu, H.; Nguyen, K.; Royce, T.; Qian, J.; Nelson, K.; Snyder, M.; Gerstein, M. *Nucleic Acids Res.* **2007**, *35*, e8.

(15) Nelson, P. T.; Baldwin, D. A.; Scearce, L. M.; Oberholtzer, J. C.; Tobias, J. W.; Mourelatos, Z. *Nat Meth.* **2004**, *1*, 155-161.

(16) Jin, Z.; Geissler, D.; Qiu, X.; Wegner, K. D.; Hildebrandt, N. *Angew. Chem. Int. Ed.* **2015**, *54*, 10024-10029.

(17) Qiu, X.; Hildebrandt, N. *Acs Nano.* **2015**, *9*, 8449-8457.

(18) Zhang, H.; Liu, Y.; Gao, J.; Zhen, J. *Chem. Commun.* **2015**, *51*, 16836-16839.

(19) Hou, T.; Li, W.; Liu, X.; Li, F. *Anal. Chem.* **2015**, *87*, 11368-11374.

(20) Cheng, F. F.; He, T. T.; Miao, H. T.; Shi, J. J.; Jiang, L. P.; Zhu, J. J. *Acs Appl. Mater. Inter.* **2015**, *7*, 2979-2985.

(21) Zhang, P. H.; He, Z. M.; Wang, C.; Chen, J. N.; Zhao, J. J.; Zhu, X. N.; Li, C. Z.; Min, Q. H.; Zhu, J. J. *Acs Nano* **2015**, *9*, 789-798.

(22) Torrente-Rodríguez, R.M.; Campuzano, S.; López-Hernández, E.; Montiel, V.R.-V.; Barderas, R.; Granados, R.; SánchezPuelles, J.M.; Pingarrón, J.M. *Biosens. Bioelectron.* **2014**, *66,* 385-391

(23) Bettazzi, F.; HamidAsl, E.; Esposito, C.; Quintavalle, C.; Formisano, N.; Laschi, S.; Catuogno, S.; Iaboni, M.; Marrazza, G.; Mascini, M.; Cerchia, L.; De Franciscis, V.; Condorelli, G.; Palchetti, I.; Anal. Bioanal. Chem. **2013**, *405*, 1025-1034.

(24) Park, S.; Singh, A.; Kim, S.; Yang, H. *Anal. Chem.* **2014**, *86*, 1560-1566.

(25) Degliangeli, F.; Kshirsagar, P.; Brunetti, V.; Pompa, P. P.; Fiammengo, R. *J. Am. Chem. Soc.* **2014**, *136*, 2264-2267.

(26) Li, S.; Xu, L.; Ma, W.; Wu, X.; Sun, M.; Kuang, H.; Wang, L.; Kotov, N. A.; Xu, C. *J. Am. Chem. Soc.* **2016**, *138*, 306-312.

(27) Zhou, X.; Cao, P.; Zhu, Y.; Lu, W.; Gu, N.; Mao, C. *Nat. Mater.* **2015**, *14*, 1058-1064.

(28) Li, J.; Zheng, C.; Cansiz, S.; Wu, C.; Xu, J.; Cui, C.; Liu, Y.; Hou, W.; Wang, Y.; Zhang, L.; Teng, I. t.; Yang, H.-H.; Tan, W. *J. Am. Chem. Soc.* **2015**, *137*, 1412-1415.

(29) Yang, H.; Xia, Y. *Adv. Mater.* **2007**, *19*, 3085-3087.

(30) Shin, J.; Choi, S.-J.; Lee, I.; Youn, D.-Y.; Park, C. O.; Lee, J.-H.; Tuller, H. L.; Kim, I.-D. *Adv. Funct. Mater.* **2013**, *23*, 2357-2367.

(31) Xia, Z.; Wang, S.; Jiang, L.; Sun, H.; Liu, S.; Fu, X.; Zhang, B.; Su, D. S.; Wang, J.; Sun, G. *Sci. Rep.* **2015**, 2045-2322.

(32)Mu, R. T.; Fu, Q. A.; Xu, H.; Zhang, H. I.; Huang, Y. Y.; Jiang, Z.; Zhang, S. O.; Tan, D. L.; Bao, X. H. *J. Am. Chem. Soc.* **2011**, *133*, 1978-1986.

(33)Beyhan, S.; Sahin, N. E.; Pronier, S.; Leger, J. M.; Kadirgan, F. *Electrochim. Acta.* **2015**, *151*, 565-573.

(34)Hou, D. M.; Zhou, W. J.; Liu, X. J.; Zhou, K.; Xie, J.; Li, G. Q.; Chen, S. W. *Electrochim. Acta.* **2015**, *166*, 26-31.

(35) Lai, G.; Wu, J.; Ju, H.; Yan, F. *Adv. Funct. Mater.* **2011**, *21*, 2938-2943.

(36) Dong, H.; Yan, F.; Ji, H.; Wong, D. K. Y.; Ju, H. *Adv. Funct. Mater.* **2010**, *20*, 1173-1179.

(37) Vayssilov, G. N.; Lykhach, Y.; Migani, A.; Staudt, T.; Petrova, G. P.; Tsud, N.; Skála, T.; Bruix, A.; Illas, F.; Prince, K. C.; Matolín, V. r.; Neyman, K. M.; Libuda, J. *Nat Mater.* **2011**, *10*, 310-315.

(38) Ho, V. T. T.; Pan, C.-J.; Rick, J.; Su, W.-N.; Hwang, B.-J. *J. Am. Chem. Soc.* **2011**, *133*, 11716-11724.

(39) Kudernatsch, W.; Peng, G.; Zeuthen, H.; Bei, Y.; Merte, L. R.; Lammich, L.; Besenbacher, F.; Mavrikakis, M.; Wendt, S. *Acs Nano.* **2015**, *9*, 7804-7814.

(40)Dong H.; Jin S.; Ju H.; Hao, K.; Xu, L.; Lu, H.; Zhang, X. *Anal. Chem.* **2012**, *84*, 8670-8674.

(41)Dong, H.; Meng, X.; Dai, W.; Cao, Y.; Lu, H.; Zhou, S.; Zhang, X. *Anal. Chem.* **2012**, *87*, 4334-4340.

(42) Kou, R.; Shao, Y.; Mei, D.; Nie, Z.; Wang, D.; Wang, C.; Viswanathan, V. V.; Park, S.; Aksay, I. A.; Lin, Y.; Wang, Y.; Liu, J. *J. Am. Chem. Soc.* **2011**, *133*, 2541-2547.

(43) Ou, D. R.; Mori, T.; Togasaki, H.; Takahashi, M.; Ye, F.; Drennan, J. *Langmuir* **2011**, *27*, 3859-3866.

(44) Ahn, H.-J.; Choi, H.-C.; Park, K.-W.; Kim, S.-B.; Sung, Y.-E. *J. Phys. Chem. B.* **2004**, *108*, 9815-9820.

(45) Shi, L.; Deng, G.-M.; Li, W.-C.; Miao, S.; Wang, Q.-N.; Zhang, W.-P.; Lu, A.-H. *Angew. Chem. Int. Ed.* **2015**, *54*, 13994-13998.

(46) Hull, R. V.; Li, L.; Xing, Y. C.; Chusuei, C. C. *Chem. Mater.* **2006**, *18*, 1780-1788.

(47) Zhao, S.; Wangstrom, A. E.; Liu, Y.; Rigdon, W. A.; Mustain, W. E. Electrochim. Acta. **2015**, *157*, 175-182.

(48) Rana, M.; Chhetri, M.; Loukya, B.; Patil, P. K.; Datta, R.; Gautam, U. K. *ACS. Appl. Mater. Inter.* **2015**, *7*, 4998-5005.

(49) Jin, S.; Chen, M.; Dong, H.; He, B.; Lu, H.; Su, L.; Dai, W.; Zhang, Q.; Zhang, X. *J. Power Sources*. **2015**, *274*, 1173-1179.

(50) Attal, S.; Thiruvengadathan, R.; Regev, O. *Anal. Chem.* **2006**, *78*, 8098-8104.

(51) Lan, G.-Y.; Chen, W.-Y.; Chang, H.-T. *Biosens. Bioelectron.* **2011**, *26*, 2431-2435.

(52) Wang, Q.; Li, Q.; Yang, X.; Wang, K.; Du, S.; Zhang, H.; Nie, Y. *Biosens. Bioelectron.* **2016**, *77*, 1001-1007.

(53) Ru-Dong, L.; Qian, W.; Bin-Cheng, Y.; Bang-Ce, Y. *Biosens. Bioelectron.* **2016**, *77*, 995-1000.

(54) Zhou, X.; Cao, P.; Tian, Y.; Zhu, J. *J. Am. Chem. Soc.* **2010**, *132*, 4161-4168.

(55) Liao, Y.; Huang, R.; Ma, Z.; Wu, Y.; Zhou, X.; Xing, D. *Anal. Chem*. **2014**, *86*, 4596 -4604.

(56) Yin, B. C.; Liu, Y. Q.; Ye, B. C. *J. Am. Chem. Soc*. **2012**, *134*, 5064-5067.

TOC

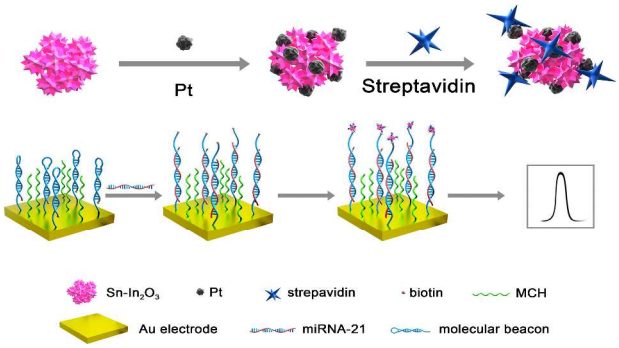
Pt
Streptavidin
Sn-In2O3
Pt
strepavidin
biotin
MCH
Au electrode
miRNA-21
molecular beacon